Exceptions to the temperature–size rule: no Lilliput Effect in end-Permian ostracods (Crustacea) from Aras Valley (northwest Iran)

by PAULINA S. NÄTSCHER[1],[*] , JANA GLIWA[2],[3] , KENNETH DE BAETS[1],[4] , ABBAS GHADERI[5] *and* DIETER KORN[2]

[1]Geozentrum Nordbayern, Friedrich-Alexander-University Erlangen-Nürnberg, Erlangen, Germany, paulina.naetscher@fau.de, k.de-baets@uw.edu.pl
[2]Museum für Naturkunde, Leibniz Institute for Research on Evolution and Biodiversity, Berlin, Germany, jana.gliwa@fu-berlin.de, dieter.korn@mfn.berlin
[3]Institute of Geological Sciences, Palaeontology Section, Freie Universität Berlin, Berlin, Germany
[4]Institute of Evolutionary Biology, Faculty of Biology, University of Warsaw, Warsaw, Poland
[5]Department of Geology, Faculty of Science, Ferdowsi University of Mashhad, Mashhad, Iran, aghaderi@um.ac.ir
*Corresponding author

Abstract: The body size of marine ectotherms is often negatively correlated with ambient water temperature, as seen in many clades during the hyperthermal crisis of the end-Permian mass extinction (*c.* 252 Ma). However, in the case of ostracods, size changes during ancient hyperthermal events are rarely quantified. In this study, we evaluate the body size changes of ostracods in the Aras Valley section (northwest Iran) in response to the drastic warming during the end-Permian mass extinction at three taxonomic levels: class, order, species. At the assemblage level, the warming triggers a complete species turnover in the Aras Valley section, with larger, newly emerging species dominating the immediate post-extinction assemblage for a short time.

Individual ostracod species and instars do not show dwarfing or a change in body size as an adaptation to the temperature stress during the end-Permian crisis. This may indicate that the ostracods in the Aras Valley section might have been exceptions to the temperature–size rule (TSR), using an adaptation mechanism that does not involve a decrease in body size. This adaptation might be similar to the accelerated development despite constant instar body sizes that can be observed in some recent experimental studies of ostracod responses to thermal stress.

Key words: Permian–Triassic, Ostracoda, body size, mass extinction, Aras Valley section.

DURING the end-Permian Period, massive CO_2 emissions caused by the Siberian Traps accumulated in the Earth's atmosphere, eventually increasing sea surface temperatures to almost 40°C in the earliest Triassic (Joachimski *et al.* 2012, 2022; Sun *et al.* 2012; Schobben *et al.* 2014; Gliwa *et al.* 2022). This caused deoxygenation of seawater (Song *et al.* 2014; Schobben *et al.* 2020) and ocean acidification (Clarkson *et al.* 2015; Jurikova *et al.* 2020). The environmental crisis caused the largest extinction in the Phanerozoic (Burgess *et al.* 2017), with extinction rates of marine species higher than 80% (Sepkoski *et al.* 1981; Sepkoski 1984; Payne & Clapham 2012; Stanley 2016).

The Aras Valley section in northwestern Iran exposes a detailed succession of end-Permian strata and allows an insight into the environmental perturbations (Ghaderi 2014; Gliwa *et al.* 2020). The succession of deep-shelf sediments reaches from the Wuchiapingian to the Griesbachian and is complete without noticeable stratigraphic gaps; it documents a rather stable bathymetric position.

Ostracods were sampled across the Permian–Triassic boundary (Gliwa *et al.* 2021). A subset of the sampled ostracods from the Aras Valley section was used to measure oxygen isotope ratios for determining palaeo-seawater temperatures in this region (Gliwa *et al.* 2022) (Fig. 1A). This allows us to test for a direct correlation between the temperatures experienced by the ostracods and their body size.

The body size of organisms is a character that is easily measurable and therefore regularly studied both in ecological and palaeobiological studies (De Baets *et al.* 2022). Body size is not only convenient to document, but can provide information about the physiological performance of an animal in a changing environment (Calosi *et al.* 2019; Kiessling *et al.* 2023). In marine ectotherms, many studies of past and present organisms have found that environmental crises, especially those caused by climate warming, were often associated with the presence of smaller organisms. In the fossil record, this size shift is
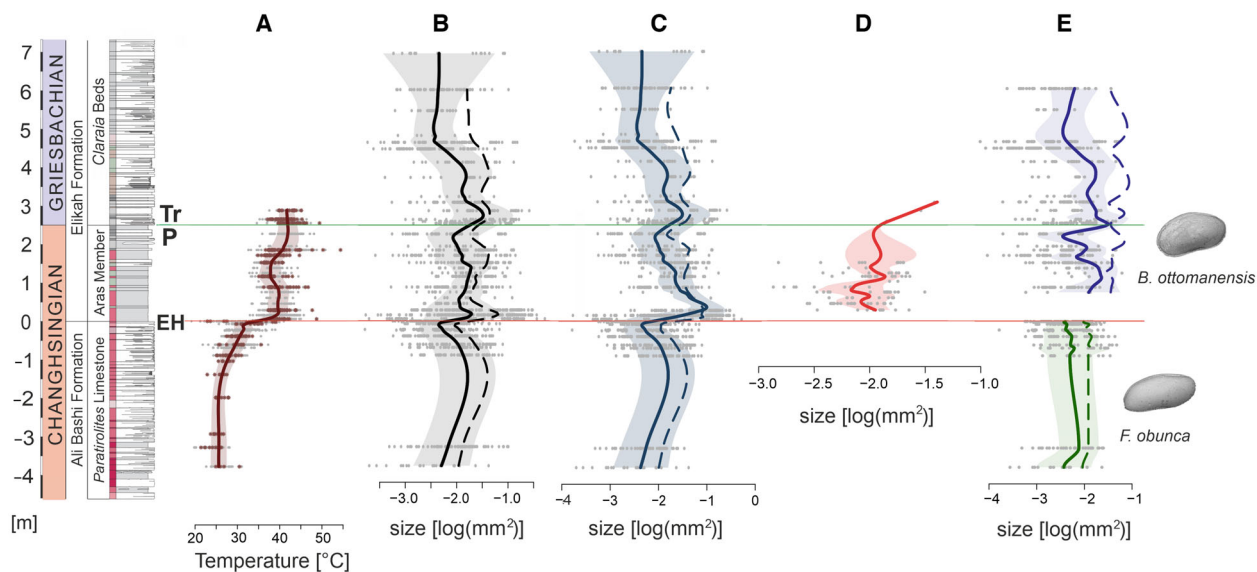
FIG. 1. Sedimentary profile of the Aras Valley section (northwest Iran) on the left, with a lower, red horizontal line indicating the extinction horizon (EH) and an upper, green line at the Permian–Triassic boundary. A, the loess-smoothed mean calculated temperature derived from oxygen isotope measurements of the ostracod carapaces with the red shading representing the loess-smoothed SD; red stars show the original data from Gliwa *et al.* (2022), grey dots are the interpolated data used in this study. B–E, the loess-smoothed median body size with the shaded area representing loess-smoothed median absolute deviation (MAD) and grey points are the raw body size data of the: B, full assemblage; C, Order Podocopida; D, Order Platycopida; E, species body size of *B. ottomanensis* (blue at the top) and *F. obunca* (green at the bottom). The dashed lines in B, C and E represent loess-smoothed body size curves of the median valve size of the A-1 instars.

referred to as the 'Lilliput Effect' (Urbanek 1993). While the original definition of this term described the decrease in body size of a surviving species-level taxon during a crisis interval (Urbanek 1993) (Lilliput Effect *s.s.*), size changes on higher taxonomic levels, such as through size-selective extinction or origination of taxa, are now also referred to as the 'Lilliput Effect *s.l.*' (Twitchett 2007). The 'Lilliput Effect *s.s.*' is usually observed as stunting of adult specimens (e.g. Rita *et al.* 2019; Nätscher *et al.* 2021). Even though this is more difficult to research in the fossil record (Twitchett 2007), it is frequently observed in modern ecological studies. In these, a negative correlation between ambient temperature and adult body size was established as the 'temperature–size rule', which describes accelerated growth and development at early life stages, with maturity being reached sooner and at a smaller size than normal (Atkinson 1994; Atkinson & Sibly 1997; Angilletta *et al.* 2004). This effect is confounded by the linear relationship between temperature and metabolic rate in ectotherms, which becomes critical as soon as the rising oxygen supply cannot be met anymore (e.g. Deutsch *et al.* 2022).

A decrease in adult body size has frequently been referred to as one of the universal responses of modern ectotherms to climate warming (Daufresne *et al.* 2009; Ohlberger 2013; Calosi *et al.* 2019), alongside poleward

migration (Reddin *et al.* 2018) and shifts in phenological events (Kordas *et al.* 2011; Poloczanska *et al.* 2016). Although several interacting causes and consequences of warming, like increased atmospheric pCO_2 and scarcity of food resources, have been proposed to stunt or modify growth processes in marine ectotherms, the effect is so universally linked to temperature, which it is commonly referred to as the temperature–size rule (TSR) (Atkinson 1994; Ohlberger 2013). Leading up to and following the end-Permian mass extinction, a Lilliput Effect can be recognized in many marine clades, such as foraminifera (Song *et al.* 2011; Feng *et al.* 2020), bivalves and gastropods (Twitchett 2007), brachiopods (He *et al.* 2007; Zhang *et al.* 2016) and conodonts (Luo *et al.* 2006, 2008). A recent study of ammonoids from north-western and central Iran has also found a Lilliput Effect *s.l.*, where the sampled taxa become smaller towards the extinction (Kiessling *et al.* 2018), corresponding to the gradual warming (Gliwa *et al.* 2022).

There is no universal evidence for the TSR in ostracods. There are several studies on Recent ostracods, where distinguishing instars is much easier than in fossils; they show a negative correlation between body size and temperature (Martens 1985; Kamiya 1988; Majoran *et al.* 2000; Cronin *et al.* 2005; Hunt & Roy 2006; Hunt *et al.* 2010; Yamaguchi *et al.* 2012). Majoran *et al.* (2000)

showed that size changes in experiments were particularly pronounced in the larger instars A and A-1 when treated with higher temperature. According to Martens (1985), there are no A or A-1 specimens in either the lowest or the highest temperature treatment, but younger instars did show a size change. Other studies even showed seasonal variation in the body size of an ostracod species with smaller adult sizes during warm summer months (Kamiya 1988; Cronin *et al.* 2005). Several species of deep-sea ostracods are also known to inversely track temperature throughout the entire Cenozoic (Hunt & Roy 2006; Hunt *et al.* 2010). Finally, another fossil study shows a dwarfing of ostracods across the Paleocene–Eocene Thermal Maximum (PETM) associated with increased temperature, ocean acidification and a lack of ideal feeding conditions (Yamaguchi *et al.* 2012).

In some studies, ostracods were not observed to reduce in size in response to increasing temperature. Instead, their developmental rate speeded up and the time intervals between moulting became shorter (e.g. Latifa 1987). This process caused ostracods to reach maturity much earlier than in colder water; however, the size of the instars in the high-temperature treatment did not differ significantly from their cold-water counterparts (Aguilar-Alberola 2013; Liberto *et al.* 2014).

Concerning the end-Permian mass extinction specifically, two studies have reported a Lilliput Effect in ostracods (Chu *et al.* 2015a; Forel *et al.* 2015). However, Chu *et al.* (2015a) observed size patterns that indicate a Lilliput effect *s.l.*, with smaller species of freshwater ostracods dominating after the extinction horizon, rather than the dwarfing within individual species (Chu *et al.* 2015a, 2015b; Forel & Crasquin 2015), similar to that reported in ammonoids (Kiessling *et al.* 2018). Forel *et al.* (2015) considered body sizes on the instar level in two podocopid ostracod species from the Elikah River section in the Alborz Mountains of northern Iran, which is located 600 km southwest of the Aras Valley section and represents a shallow water environment (Forel *et al.* 2015). The results of this study suggested that, in both species, each instar was much smaller in the Triassic than it was in the Permian. However, the study consisted of only two time-bins (late Permian and Early Triassic), the second of which was represented only by very small sample sizes; therefore, further study is required.

Even though the TSR is defined very generally for ectotherms, there appear to be clear exceptions from the rule, some of which are not yet fully understood. Studying the patterns in ecological traits to identify which organisms obey ecological rules and which are exempt, is an important step to learning differences in sensitivities of marine clades to future climate change (Calosi *et al.* 2019). In this study, we investigate the body size pattern of ostracods from the Permian–Triassic Aras Valley section in northwest Iran at the assemblage, order, species and instar level (Nätscher *et al.* 2023, data D1). We correlate these with palaeoenvironmental proxies, including the ambient temperature estimations derived directly from oxygen isotope measurements of ostracod calcite of specimens from the Aras Valley samples (Gliwa *et al.* 2021, 2022) (Fig. 1) (Nätscher *et al.* 2023, data D2).

GEOLOGICAL BACKGROUND

The ostracod body size data used in this study resulted from a stratigraphic study of the Aras Valley section in northwestern Iran (West Azerbaijan Province, 39.0154°N, 45.4345°E) that is close to the Dorasham, Ali Bashi and Zal sections, which are all located near the Iranian/Azerbaijanian border (Gliwa *et al.* 2020). The Aras Valley section comprises a more than 34-m-thick succession of sedimentary rocks recording the Wuchiapingian, the Changhsingian and the early Griesbachian stages; there are no noticeable stratigraphic gaps, as all expected conodont zones are present here (Ghaderi 2014). This allows for a very precise correlation of the Permian–Triassic boundary with the GSSP section (Gliwa *et al.* 2020).

In late Permian times, the Aras Valley locality had a position close to the equator, on the northern shelf of the Cimmerian microcontinent that separated Neotethys and Palaeotethys (Stampfli & Borel 2002, 2004; Muttoni *et al.* 2009a, 2009b). In ascending order, the rock succession that is exposed in the Aras Valley section consists of three principal units: (1) the Wuchiapingian Julfa Formation; (2) the Changhsingian Ali Bashi Formation, with the Zal Member and the *Paratirolites* Limestone that records the extinction horizon at its upper surface; (3) the Elikah Formation that spans from the latest Changhsingian Aras Member ('Boundary Clay') to the early Griesbachian *Claraia* Beds above the Permian–Triassic boundary (Ghaderi *et al.* 2014; Gliwa *et al.* 2020, 2021). Ostracods were sampled in 59 horizons spanning the 4.73-m-thick *Paratirolites* Limestone, the 3.30-m-thick Aras Member, and the lowest 5 m of the *Claraia* Beds (Ghaderi 2014, Gliwa *et al.* 2020, 2021).

The depositional environment of the *Paratirolites* Limestone was interpreted as characteristic of deep shelf deposits in the dysphotic zone with low terrigenous input and consistently oxic conditions (Leda *et al.* 2014; Gliwa *et al.* 2020). There is evidence for low sedimentation rates and early lithification processes in the uppermost part of the *Paratirolites* Limestone, whose top bedding surface coincides with the main pulse of the end-Permian mass extinction (EPME) (Gliwa *et al.* 2020). It is likely that this enabled the settlement accumulation of sponges (Gliwa *et al.* 2020), as also known from other time equivalent sections (Friesenbichler *et al.* 2018; Heindel *et al.* 2018;

Foster *et al.* 2020). However, the hardground does not represent a very long time interval, but developed due to early lithification processes of the sediment. The bathymetric position of the section probably did not change from the *Paratirolites* Limestone to the post-extinction Aras Member, which was also deposited in a low-energy outer shelf setting (Gliwa *et al.* 2020). However, there is a sharp decline in skeletal carbonate production, leading to lower abundances of fossils, as well as to a change in lithology from the carbonate-rich *Paratirolites* Limestone to the Aras Member that is dominated by shale deposits (Gliwa *et al.* 2020). For the *Claraia* Beds, a shallowing-upward trend can be observed in the Ali Bashi and Zal sections (Leda *et al.* 2014; Gliwa *et al.* 2020).

MATERIAL AND METHOD

Material

Limestone and marly limestone rock samples were processed using hot acetolysis following Crasquin-Soleau & Kershaw (2005). Shale samples were dissolved in water. Each sample was wet-sieved, with the smallest sieve having a mesh size of 0.063 mm. The majority of ostracods in the Aras Valley section have smooth carapaces without ornamentation. In addition, carapaces were filled with spar, which could not be removed without destroying them. Therefore, the taxonomic identification to species level was not based on internal structures, but rather involved traditional morphological measurements and features of the outside of the carapace, such as the hinge, carapace length and height as well as their proportions, as described in Gliwa *et al.* (2021). The resulting dataset consists of 2076 ostracod specimens from four orders (Podocopida, Palaeocopida, Platycopida and Myodocopida) (Nätscher *et al.* 2023, data D1).

For species-specific analyses, we only used the two species that have sample sizes larger than n = 20 in at least five horizons (*Fabalicypris obunca*, *Bairdiacypris ottomanensis*) (Fig. 2). *Fabalicypris obunca* is only found in the *Paratirolites* Limestone and does not reappear above the extinction horizon. *Bairdiacypris ottomanensis* first appears at 0.75 m above the extinction horizon and ranges across the Permian–Triassic boundary up to the end of the section at 6.00 m.

Statistical methods

Instar classification . To classify the size data of *B. ottomanensis* and *F. obunca* into their instars (moulting stages), we used the mclust package in R (v.6.0.0; Scrucca *et al.* 2016; Fraley *et al.* 2022) to test and fit a Gaussian

Fm.	Mb.	Position [cm]	N	A	A-1	A-2	A-3	A-4	A-5	
Elikah Formation	*Claraia* Beds	605	48	1	4	3	12	16	12	*Bairdiacypris ottomanensis*
		550	7	0	0	1	0	4	2	
		467	56	4	8	4	10	16	14	
		450	85	0	3	8	8	23	43	
		415	20	2	3	4	4	4	3	
		375	10	0	0	6	0	2	2	
		325	8	0	1	1	3	2	1	
		310	67	0	17	6	30	8	6	
		288	17	0	3	6	4	3	1	
		265	13	0	3	4	0	1	5	
		260	11	3	3	3	1	1	0	
		255	47	5	18	3	13	8	0	
	Aras Member	227	26	0	0	5	5	11	5	
		195	11	0	1	1	3	4	2	
		185	57	4	21	5	21	5	1	
		171	53	1	4	4	12	15	17	
		152	52	6	11	7	17	8	3	
		138	12	1	4	3	3	1	0	
		125	4	1	1	0	1	1	0	
		116	2	0	1	0	1	0	0	
		88	48	1	10	5	14	16	2	
		75	4	0	2	0	0	1	1	
Ali Bashi Formation	*Paratirolites* Limestone	−1	68	0	13	29	16	10		*Fabalicypris obunca*
		−3	42	3	11	12	10	6		
		−8	40	2	9	18	8	3		
		−23	48	2	13	15	11	7		
		−25	23	0	6	9	5	3		
		−40	75	10	18	20	16	11		
		−62	19	5	1	7	3	3		
		−70	17	4	4	4	4	1		
		−90	23	3	4	10	5	1		
		−330	33	4	12	8	4	5		
		−380	18	1	5	4	3	5		

FIG. 2. Abundances of the instars of the two most abundant species *B. ottomanensis* and *F. obunca* by the bed. Grey numbers indicate samples with n < 3. These samples were not used in pairwise Wilcoxon tests and the palaeo trend detection analyses of instar sizes.

finite mixture model on the length and height measurements of the ostracod carapaces (Hunt & Chapman 2001). As we have prior information on the ideal shape and distribution of ostracod instar groups, we tested the two spherical (EII (equal volume), VII (unequal volume)) and four diagonal models (EEI (equal volume and shape), VEI (varying volume, equal shape), EVI (equal volume, varying shape), VVI (varying volume and shape)), with the pre-defined number of instar groupings of six for *B. ottomanensis* and five for *F. obunca*. These numbers of instar groupings are derived from Gliwa *et al.* (2021), which shows that the same specimens of *B. ottomanensis* that are used in this study, have six instars present, and all examined *Fabalicypris* species in the Aras Valley section have five instars preserved (Gliwa *et al.* 2021). In both of these well-sampled species, the diagonal VEI (varying volume, equal shape) model has the lowest Bayesian information criterion (BIC) and is therefore the most parsimonious model for classifying the instar groupings (Fig. S1). Therefore, we ran the mclust function with

this model on the size data of the 25 other species with ten or more specimens present in the data to classify their instars. In order to avoid species that show signs of severe post-mortem transport (taphocoenosis), we excluded eight ostracod species, for which the algorithm could only identify one or two instar clusters (Boomer *et al.* 2003). These are: *Bairdia* sp. 5; *Bairdiacypris kathleenae*; *Carinaknightina hofmanni*; *Cavellina hairapetani*; *Kempfina qinglaii*; *Liuzhinia antalyaensis*; *Buregia*? sp.; and *Microcheilinella* sp. 1. With *Praezabythocypris pulchra* and *Praezabythocypris* cf. *pulchra* pooled and defined as one species, we could identify instar clusters of 18 species, including *F. obunca* and *B. ottomanensis* (Fig. S4).

Body size through time and evolutionary trends. We calculated the approximate valve area of each ostracod, which we referred to as body size in this study for the sake of simplicity:

$$\text{Approximate valve area} = (\text{height} \times \text{length}) \times (\pi/4)$$

We calculated the median size and median absolute deviation of each bed for the full assemblage, the most abundant ostracod order Podocopida, the two most abundant species (*B. ottomanensis*, *F. obunca*), and the two species' individual instars. To test for changes in body size between consecutive beds in all aforementioned taxonomic subsets of the data, we used pairwise Wilcoxon rank sum tests. We used the method proposed by Holm (1979) to correct p-values for small and uneven sample sizes and defined the alpha level for significance at 0.05 throughout all analyses. To avoid a bias from extremely low sample sizes, we only included beds with a minimum sample size threshold of at least three specimens.

To detect trends in the median log-transformed instar body sizes of the two species *F. obunca* and *B. ottomanensis*, we used the paleoTS package in R (v.0.5.2; Hunt 2019). For each instar group of these subsets, we tested five different evolutionary models: (1) general random walk (GRW); (2) unbiased random walk (URW); (3) stasis; (4) a covariate tracking model with $\delta^{13}C$ values (Gliwa *et al.* 2020) model; and (5) a covariate tracking model with the Aras Valley ostracod temperature values (Gliwa *et al.* 2022) (Tables S4, S5). Because the environmental proxies are sampled on shorter timescales than *B. ottomanensis*, we removed beds above 2.88 m due to a lack of temperature estimates beyond this point.

Assemblage turnover and body size. We used an approach initially developed by Rego *et al.* (2012), and adapted by Rita *et al.* (2019), to assess body size dynamics of the entire ostracod assemblage (Fig. 3; Table S1) (Nätscher
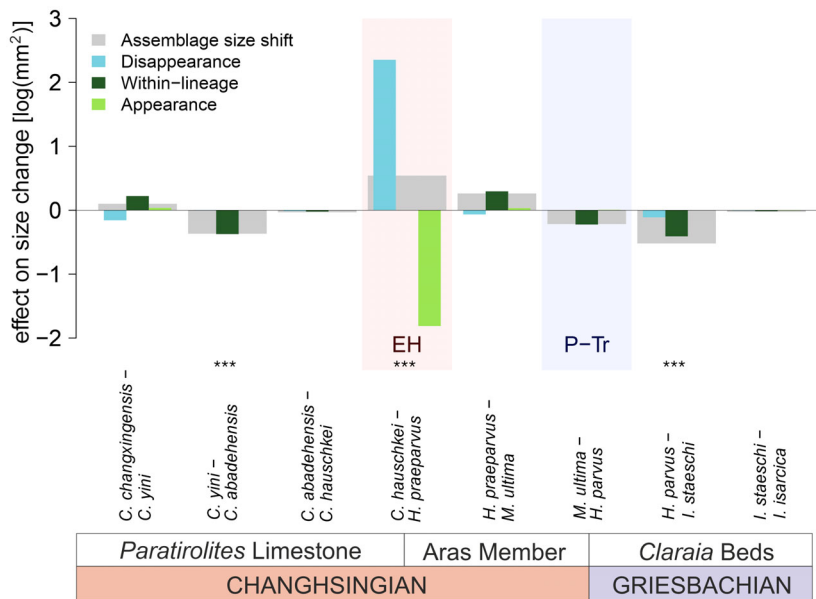

FIG. 3. Results of the Rego approach (Rego *et al.* 2012), showing body size changes of the ostracod assemblage between consecutive conodont zones and the contributions of within-species size changes (dark green), as well as species appearances (light green) and disappearances (light blue) to the overall size pattern. The red rectangle in the background signifies the extinction horizon, the blue rectangle shows the Permian–Triassic boundary. Three changes are highly significant: *C. yini – C. abadehensis*; *C. hauschkei – H. praeparvus* (EH); *H. parvus – I. staeschei*. The two decreases in body size (*C. yini – C. abadehensis*, *H. parvus – I. staeschei*) are mainly triggered by within-species changes, while the size increase across the extinction horizon is caused by a full species turnover, with the new species being significantly bigger than the ones that disappear.

et al. 2023, data D3). This method quantifies the contribution of within-lineage size changes, as well as species appearance or disappearance effects to the overall size pattern across zone boundaries. This helps distinguish between a Lilliput Effect *s.l.* and a Lilliput Effect *s.s.* As this method is highly dependent on the importance of boundary-crossing species, we did not analyse this at the bed level, but on conodont zone level to obtain more reliable results with minimal impact of irregular sampling. All species were included in this analysis, as less abundant species are also crucial for understanding the impact of appearances and disappearance on the assemblage-scale body size patterns.

We also assessed changes in relative abundance of the four occurring ostracod orders (Fig. 4; areaplot v.1.2.3; Magnusson 2022), which correspond to different dietary strategies. Almost all platycopids and all myodocopids have the possibility of suspension feeding, while podocopids are exclusively grazers, detritus feeders or predatory (e.g. Whatley 1991).

Correlation with palaeoenvironmental proxies . We used three different proxies for the biotic and abiotic palaeoenvironment, to test for correlations between the environment and the ostracods' body size.

To relate ostracod body sizes to local temperature estimates, we used the temperature data from Gliwa *et al.* (2022) (Fig. 1) (Nätscher *et al.* 2023, data D2). The temperature values in that study were reconstructed from $\delta^{18}O$ measurements of 605 diagenetically unaffected ostracod carapaces from the Aras Valley section using the equation of Kim & O'Neil (1997) (Gliwa *et al.* 2022). The minimal influence of diagenesis in the ostracod carapaces was secured by: (1) the stable low-Mg calcite composition of the ostracod carapace (Brand & Veizer 1981); (2) the
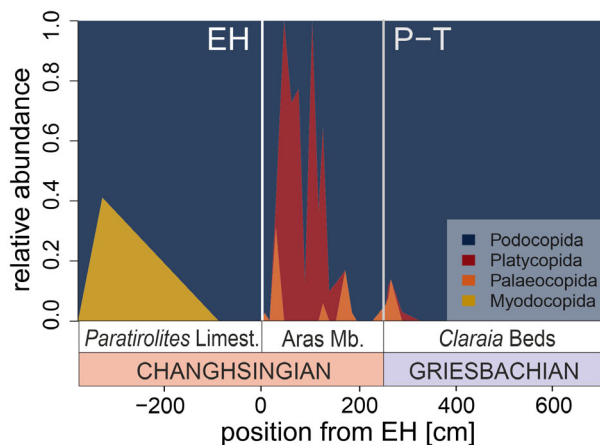
lack of signs indicating subaerial exposure throughout the section; and (3) a conodont alteration index between 1 and 1.5 (Königshof 1992), an indication of low thermal overprinting in the burial process (Gliwa *et al.* 2022). Most of the temperature data come from the two most abundant species, *B. ottomanensis* and *F. obunca*, but the record of temperature estimates stops 2.88 m above the extinction horizon. Since the temperature dataset only represents 23 beds, compared to 31 beds in the ostracod occurrence data up to the end of the temperature curve at 2.88 m (41 beds in total) (Gliwa *et al.* 2022), we linearly interpolated temperature values for the missing beds so as not lose more ostracod size data in analyses that include both size and temperature. To assign a temperature value to beds with missing data, we calculated the mean temperature of the two beds before and after the missing sample. Where there were several beds with missing data between two beds with temperature estimates, we divided the temperature difference between the two beds with data by the number of missing beds between them plus 1, and used the result as the temperature difference between the consecutive beds. To preserve the maximal amount of ostracod size data in analyses, we also extended the sample sizes of the temperature data for each bed, as there were many fewer temperature observations than size measurements. For this purpose, we simulated normally distributed data based on the mean and standard deviation of the calculated temperature of each bed, but with the sample size of the body size data. For beds, where the mean temperature was interpolated between beds with data, we assigned the mean of the standard deviations of all sampled beds, as their standard deviation for the simulation step. Both, the original temperature data as well as the interpolated data, which were used for analyses, can be seen in Figure 1A. The gradual warming from 1.5 m below the extinction horizon culminates in a rapid increase in temperature across the extinction. After a temperature drop from 0.88 to 1.16 m, the temperature values quickly return to their higher levels and stay steadily high until the records end at 2.88 m.

To correlate ostracod body size patterns with changes in primary productivity, we reverse engineered carbon isotope data (Fig. S2) from Gliwa *et al.* (2020) using WebPlotDigitizer (Rohatgi 2022). Corrected-in-bin diversity (Alroy 2008) was calculated using the divDyn function from the R package divDyn (v.0.8.1; Kocsis *et al.* 2019, 2021), in order to assess whether body size changes of ostracods were impacted by the diversity, and by extension the competition for resources (e.g. disaster taxa) (Fig. S2).

To investigate whether body size is correlated with the aforementioned palaeoenvironmental proxies, we first tested for correlation between the independent variables using corrplot (v.0.92; Wei & Simko 2021). Based on the

FIG. 4. Areaplot of the relative abundances of the four ostracod orders (Podocopida, Platycopida, Palaeocopida, Myodocopida) for all sampled beds in the Aras Valley section.

results we discarded $\delta^{13}C$, which shows a high negative correlation (-0.75) with the estimated ambient temperature (Dormann *et al.* 2013) (Fig. S3), and proceeded using only the estimated ambient temperature of the ostracods and corrected sampled-in-bin richness (Alroy 2008, Kocsis *et al.* 2019).

We ran a general linear model (glm) with a Gaussian error distribution and both independent variables (temperature and diversity) on the log-transformed body size of the full ostracod assemblage and the species *F. obunca* and *B. ottomanensis*, as well as subsets containing only A-1 specimens of each of these. Because of the significant temporal autocorrelation of the residuals in these generalized linear models, we then used generalized least squares (gls) models from the nlme package in R (v.3.1-157; Crawley 2007; Groß 2010; Pinheiro *et al.* 2021) for the same subsets. This function allows for the implementation of an autoregressive (AR or p) and moving average (MA or q) component to correct for specific temporal autocorrelation in our data:

$$log(body\text{-}size) \sim temperature + diversity, correlation\,(p, q)$$

To find the appropriate autoregressive (p) and moving average (q) variables for the gls models, we tested models with either variable from 0 to 5 on the full model, which contains both temperature and diversity as variables. The best p and q variables for the assemblage all (p = 5, q = 5), assemblage A-1 (p = 2, q = 3), *F. obunca* all (p = 1, q = 1), *F. obunca* A-1 (p = 1, q = 1), *B. ottomanensis* all (p = 2, q = 3) and *B. ottomanensis* A-1 (p = 0, q = 0) models were chosen by determining the model with the lowest BIC (Table S2). We consistently used these autoregressive and moving average variables in the null model, the single variable models (temperature or corrected in-bin-diversity, respectively), and the full model with temperature and diversity. For each subset of the data (assemblage, assemblage A-1, *F. obunca*, *F. obunca* A-1, *B. ottomanensis*, *B. ottomanensis* A-1), the most parsimonious of those models for each group was determined by both AIC (Wagenmakers & Farrell 2004) and BIC, which agreed in all instances (Table S3). All statistical analyses were conducted in R (v.4.2.0; R Core Team 2013).

RESULTS

Species turnover drives post-extinction assemblage body size increase

Three significant changes in the median body size of the ostracod assemblage between successive conodont zones were recognized in the Aras Valley section (Fig. 3). One occurs below the extinction horizon, one coincides with the extinction horizon and one is above the Permian–Triassic boundary. These changes are largely due to body size fluctuations within the surviving species, except for the size increase at the extinction horizon, which is due to a complete species change without survivors (Fig. 3, Table S1).

The first significant reduction in body size occurs at the turn from the *Clarkina yini* to the *Clarkina abadehensis* Zone ($\Delta_{SI} = -0.367$ log(mm^2), $p < 0.001$). The median size of the ostracod assemblages does not change significantly in the highest part of the *Paratirolites* Limestone at the transition from the *Clarkina abadehensis* Zone to the *Clarkina hauschkei* Zone. However, the transition from the *C. hauschkei* to the *Hindeodus praeparvus – Hindeodus changxingensis* Zone (which coincides with the main EPME pulse) shows a sudden and highly significant increase in size ($\Delta_{SI} = +0.542$ log (mm^2), $p < 0.001$) with a complete species change (Fig. 3). The newly occurring species have significantly larger carapaces than the species that disappear in this horizon. Within the Aras Member, almost only species occurring in both conodont zones contribute to a slight but insignificant increase in median assemblage size ($\Delta_{SI} = +0.263$ log(mm^2)). At the transition to the *Hindeodus parvus* Zone (= Permian–Triassic boundary), there is almost no species turnover in the ostracod assemblage. The surviving species decrease slightly in body size ($\Delta_{SI} = -0.217$ log(mm^2)), but this is also not a significant change (Fig. 3). At the transition from the *Hindeodus parvus* Zone to the *Isarcicella staeschei* Zone, there is another, significant, decrease in body size ($\Delta_{SI} = -0.519$ log(mm^2), $p < 0.001$), mainly caused by a decrease in median size within species and the disappearance of some of the species from the samples. Body size remains constant in the following conodont zone.

When assessing changes between consecutive beds (samples), the median assemblage body size is fairly stable throughout the *Paratirolites* Limestone (Fig. 1B). The first, marginally significant size increase, occurs across the extinction horizon ($\Delta_{SI} = +0.770$ log(mm^2), $p = 0.012$). Between 1.71 and 2.55 m, there are three consecutive significant size fluctuations (1.71–1.85 m: $\Delta_{SI} = 0.703$ log(mm^2), $p = 0.001$; 1.85–2.27 m: $\Delta_{SI} = -0.549$ log(mm^2), $p < 0.0001$; 2.27–2.55 m: $\Delta_{SI} = 0.562$ log(mm^2), $p = 0.001$). Two more significant size decreases occur from 2.88 to 3.10 m ($\Delta_{SI} = -0.554$ log(mm^2), $p = 0.001$) and from 4.15 to 4.50 m ($\Delta_{SI} = -0.736$ log(mm^2), $p = 0.028$) (Fig. 1B).

After correcting for temporal autocorrelation, this pattern shows a slightly positive, marginally significant correlation with the corrected in-bin-diversity ($p = 0.048$) (Table S3). This positive correlation with diversity still holds, when testing for the correlation of the body size of only A-1 specimens of the assemblage with palaeoenvironmental proxies (Table S3).

Changes in assemblage composition

We recognized several changes in the relative abundance data of the ostracod orders in the data (Fig. 4). Below the extinction horizon, representatives of the order Podocopida make up 100% of the ostracod assemblage in every bed except at -3.30 m, the only bed where the order Myodocopida constitute almost half of the assemblage. The bed above the extinction horizon (0.05 m) marks the beginning of a period of volatility in the composition of the assemblage with the appearance of other ostracod orders. The 0.05 and 0.15 m layers are still dominated by the order Podocopida (97% and 100%, respectively). At 0.28 m, the Palaeocopida become abundant (31%), and the order Platycopida occurs for the first time. From 0.45 to 1.20 m, the Platycopida dominate in most samples, in some they make up 100% of the ostracods. From 1.38 m, the order Podocopida again dominates the ostracod collection with some minor (<17%) occurrences of platycopids and palaeocopids up to the sample at 3.10 m. From sample 3.25 m upwards, the composition of the assemblage returns to the same pattern as below the extinction horizon, with the order Podocopida accounting for 100% of the ostracods (Fig. 4).

As the Podocopida are mainly considered to be detritivores and grazers, while the platycopids and palaeocopids are interpreted as suspension feeders (e.g. Whatley 1991), these changes in the orders' relative abundances imply a change in the dominant feeding strategy in the studied section. Detritivorous podocopids dominate the samples until just above the extinction horizon and above the Aras Member. However, suspension-feeding palaeocopids and platycopids occur after the disappearance of podocopids slightly above the extinction horizon and dominate the assemblage from sample 0.45 m to the middle of the Aras Member (Figs 1C–D, 4). Suspension feeders are still present in the upper half of the Aras Member, but in much lower proportions than the Podocopida, which dominate the assemblage again later on.

Short-lived post-extinction assemblage of podocopids

The major changes in the assemblage composition, or dominating ostracod orders, coincide with distinct body size changes in the order Podocopida. Within this order, there is a significant size increase across the extinction horizon (Fig. 1C), where the median body size increases from -2.399 log(mm^2) to -1.650 log(mm^2) ($p = 0.021$). The next significant size change in the podocopids is a size decrease from the samples 0.28 to 0.88 m ($\Delta_{SI} = -0.715$ log(mm^2), $p < 0.001$). This is later followed by significant median body size fluctuations within the Podocopida between 0.060 log(mm^2) and 0.133 log(mm^2)

from 1.52 m above the extinction horizon to the top of the boundary clay at 2.55 m (1.52–1.71 m: $\Delta_{SI} = -0.713$ log(mm^2), $p < 0.0001$; 1.71–1.85 m: $\Delta_{SI} = +0.796$ log (mm^2), $p < 0.0001$; 1.85–2.27 m: $\Delta_{SI} = -0.547$ log(mm^2), $p < 0.0001$; 2.27–2.55 m: $\Delta_{SI} = 0.542$ log(mm^2), $p = 0.002$). Between 2.88 and 3.10 m, there is a last highly significant decrease in podocopid median body size from -1.337 log(mm^2) to -1.897 log(mm^2). After this, the size index stays between -2.414 log(mm^2) and -2.145 log (mm^2) for the rest of the sampled interval, with only a marginally significant decrease in size between 4.15 and 4.50 m above the extinction horizon.

As podocopids make up the majority of the ostracod assemblage during the warming interval, we rely on the results of the gls models of the full assemblage, which show that assemblage mean size is not correlated with temperature or diversity (Fig. 4; Table S3).

The first assemblage above the extinction horizon consists of 12 podocopid species, all of which only occur up to about 0.60 m above the extinction horizon, where podocopid body size returns to pre-extinction levels. Of these 12 species, including two species of the extinction horizon-crossing genus *Fabalicypris*, six have significantly larger carapaces than the others (Fig. S5; Table S6). These are the two *Fabalicypris* species *F.* cf. *minuta* and *F. veronicae*, as well as *Kempfina qinglaii*, *Kempfina* sp. 1, *Kempfina* sp. 2, and *Iranokirkbya brandneri* (Fig. S5; Table S6). While most species are rare immediately above the extinction horizon, with abundances below 20 individuals per species, three of these large species (*Fabalicypris* cf. *minuta*, *F. veronicae*, *Kempfina qinglaii*) are very abundant, with numbers of specimens ranging from 40 to 50 only 0.15–0.28 m above the extinction horizon. In *Fabalicypris* cf. *minuta* and *Fabalicypris veronicae*, almost all instars are present at 0.15 and 0.28 m, resembling the instar abundance pattern of moderate energy autochthonous thanatocoenosis (Boomer *et al.* 2003) (Fig. S4). This indicates that these species are still acceptable palaeoenvironmental indicators (Boomer *et al.* 2003). These large and abundant species drive the significant increase in the mean body size of podocopids across the extinction horizon.

No dwarfing within the species

For the species-level and instar-level analysis of the two most abundant podocopid species in the Aras Valley section, we used a quantitative method for classifying instars that is robust against inconsistent sampling. These are *F. obunca*, which occurs up to the extinction horizon, and *B. ottomanensis*, which emerges 0.75 m above the extinction horizon and reaches the top of the studied section (Fig. 2). In *F. obunca*, the chosen model classes the largest

instar (adults) around a mean length of 0.77 mm and width of 0.33 mm, A-1 has a mean length of 0.64 mm and width of 0.28 mm, A-2 has a mean length of 0.53 mm and width of 0.24 mm, A-3 has a mean length of 0.43 mm and width of 0.20 mm, and A-4 has a mean length of 0.35 mm and width of 0.18 mm. All consecutive instar clusters are separated by a growth factor around 1.2 (1.15–1.23), which is typical for ostracod growth, making this model a credible fit for the instars of this species (Fig. S1). The mean length and width of the six *B. ottomanensis* instars are as follows: A (length = 0.92 mm; width = 0.53 mm), A-1 (0.73 mm; 0.43 mm), A-2 (0.64 mm; 0.38 mm), A-3 (0.57 mm; 0.34 mm), A-4 (0.47 mm; 0.28 mm), A-5 (0.35 mm; 0.22 mm) (Fig. S1). The growth factor between consecutive instars in this species is less consistent, ranging from 1.12 to 1.32. Gliwa *et al.* (2021) suspected sexual dimorphism in *B. ottomanensis*. However, this should not affect our analyses, as the adults resulting from the clustering model in this study overlap exactly with the specimens identified as adults by Gliwa *et al.* (2021).

The within-species body size of *F. obunca* is stable throughout its occurrence in the section, showing no significant changes between consecutive beds (Fig. 1E). The most parsimonious of the generalized least squares models for the body size pattern of all specimens of *F. obunca* model contains a slight, positive correlation with corrected in-bin-diversity (value = 0.058, *p* = 0.313) (Table S3) after correcting for the temporal autocorrelation of all variables. However, the correlation between body size and diversity is not significant.

Even though the instar body sizes of *F. obunca* seem to become more variable after 1 m below the extinction horizon, there are no significant bed-to-bed body size changes in any instar (Fig. 5). This is confirmed in the trend detection of the instar body sizes in *F. obunca*, which show no directional trend in their body size pattern. For the adults (A), as well as A-3 and A-4 of *F. obunca*, the unbiased random walk and stasis model are the most parsimonious to explain the body size trends. Both models consistently show the same results for those three instar stages (Table S5). For the A-1 specimen body size, stasis is the best trend model, and for A-2 body size the unbiased random walk shows the best results (Table S5). Additionally, the most parsimonious generalized least squares model of instar A-1 of *F. obunca* is the null model indicating that the correlation with diversity in the full species body size pattern is probably impacted by evenness of sample sizes, which determine the availability of instars (Fig. 2).

The median species body size of *B. ottomanensis* oscillates, especially with two consecutive significant body size changes between the beds at 1.51 and 1.85 m (Fig. 1E). However, the changes in instar sizes of *B. ottomanensis*
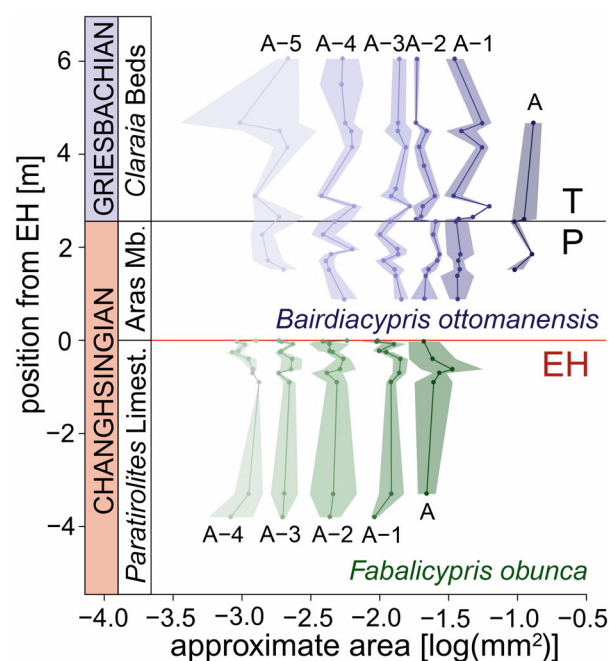
FIG. 5. Body size patterns (Median + MAD) of the individual instars of *F. obunca* (green) and *B. ottomanensis* (blue) through the Aras Valley section. Adults (A) at the larger end in darker shades, with instars becoming progressively younger towards the left (lighter shades).

are insignificant, except for a size decrease in the median size of instar A-3 above the Permian–Triassic boundary from 2.88 to 3.10 m ($\Delta_{SI} = -0.133$ log(mm^2), *p* = 0.005). As such a change cannot be observed in the other instars (Fig. 5), the body size fluctuations of the species are probably caused by varying abundances of instars (e.g. adults). The trend analysis of the individual instar size patterns of *B. ottomanensis* shows that in the adults, A-2 and A-5, the stasis and the unbiased random walk model are the most parsimonious and perform equally well (Table S4). The body size of A-2 shows a stasis pattern, while the best model for instars A-3 and A-4 is the unbiased random walk (Table S4). This indicates that none of the instars of *B. ottomanensis* show a directional body size trend. Additionally, neither the full species body size pattern, nor the body size of the instar A-1 of this species correlates significantly with either, available temperature data or sampled-in-bin diversity (Table S3).

DISCUSSION

Ostracod survival

In the Aras Valley section, the end-Permian extinction horizon coincides with the peak of a gradual increase in

calculated ambient temperature of *c.* 12°C (Gliwa *et al.* 2022) (Fig. 1A). This coincides with a complete species turnover of the ostracod assemblage at the base of the Aras Member with none of the pre-extinction species being sampled above the extinction horizon (Fig. 3). This is very different from most other Permian–Triassic boundary sections, which typically show higher survival rates, but lower diversity in the immediate post-extinction phase (Crasquin & Forel 2014; Forel *et al.* 2015; Gliwa *et al.* 2021). However, considering the abundance of ostracods in the samples below the extinction horizon and the general resilience of ostracods in high-temperature environments (Wickstrom & Castenholz 1971; Song *et al.* 2014), we think that warming was not the sole cause of these species' disappearance. Instead, we suggest climate warming as the ultimate cause of the ostracod extirpation in the Aras Valley section. A temperature rise often triggers cascading effects, such as the collapse of food webs, which probably more proximately contributed to the habitat becoming unsuitable for the species that were present before the change.

Thriving podocopid assemblage drives size increase

The stable median body size of the full ostracod assemblage during the gradual warming period leading up to the mass extinction horizon (Fig. 1B) is very different from the incremental decrease in body size of ammonoids in the same area (Kiessling *et al.* 2018). In the ammonoids, this decrease is caused by a size-selective step-by-step assemblage turnover, with the new, smaller taxa dominating (Lilliput Effect *s.l.*) Instead of the Lilliput Effect we expected, the ostracod assemblage in the Aras Valley section shows a post-extinction body size increase along with the turnover coinciding with the extinction horizon (Figs 1B, 3). This is driven by the occurrence of a completely new and diverse, but very short-lived, podocopid assemblage of which six species are characterized by significantly larger carapaces than co-occurring species. As the correlation of assemblage body size with diversity is only marginally significant (Table S3), and range-through diversity values are not available for just above the extinction horizon, we exclude the possibility of this being a typical low-diversity, high-stress assemblage. The even sampling of all available instars (Fig. S4) in many of the present species also indicates that these assemblages have not experienced a high level of post-mortem transport and can be used as a good and well-preserved indicator of the palaeoenvironment (Boomer *et al.* 2003). Finally, the high abundances of some of these species imply that this is not a struggling survival assemblage as seen in other sections, but a stable recovery assemblage (Crasquin & Forel 2014).

The majority of the species with large carapaces in this short-lived assemblage, including two abundant

Fabalicypris species, belong to the family Bairdiidae; they are adapted to many environmental conditions, from restricted to open marine settings, but usually with stable salinity and oxygen conditions (Melnyk & Maddocks 1988; Forel *et al.* 2013, 2019). They dominate the survival assemblages after the end-Permian extinction in many places, such as the nearby Elikah River section (Crasquin & Forel 2014).

After the extinction event, the establishment of species with large individuals might have been favoured by various factors (Brown & Maurer 1986; Kingsolver & Pfennig 2004). For example, if many larger predatory organisms disappeared as a result of the environmental crisis, predation pressure would have been minimized and primary consumers such as ostracods could have expanded their abundance (Forel 2013). In addition, the metabolism, and thus food utilization, of larger organisms can often be more efficient than in smaller species (Brown & Maurer 1986). It was probably a combination of the advantages of larger body size, favourable oxygen conditions in the Aras Valley section, and the adaptability of species of the family Bairdiidae to different environments that enabled this distinctive transitional assemblage to establish itself quickly in a newly vacated space and best utilize the available food resources.

Suspension feeders dominate post-extinction

Although the assemblage in the lowermost part of the Aras Member is diverse, it is very short-lived and reverts to species with smaller carapaces about 0.60 m above the extinction horizon. This transition in the lower part of the Aras Member is characterized by a change from dominant detritivorous podocopids to suspension-feeding platycopids (Figs 1C, D, 4). This pattern was often referred to as the 'platycopid signal' in the ostracod literature (Whatley 1991; Brandão & Horne 2009; Horne *et al.* 2011). The dominance of platycopid ostracods was originally interpreted as a marker for dysoxic conditions (e.g. Whatley 1991), but other studies suggested it is rather caused by oligotrophic conditions (Horne *et al.* 2011). Most of these studies were, however, not based on quantitative testing. Our discussion and interpretations are based on the most recent facies analysis of the Aras Valley section, which bears no lithological or ecological signs of dysoxia (Gliwa *et al.* 2020). Detailed investigation of the 'platycopid signal' and its cause, however, is beyond the scope of our study, therefore we do not want to read a specific environmental signal into this shift in relative abundance in the feeding strategy of ostracods. However, we assume that it is related to the full range of environmental and ecological changes brought about by the warming and mass extinction at this time.

Limitations with assigning fossil ostracod instars

Regarding the interpretation of body size at the instar level, we would first like to address the conservative nature of our method for clustering instar elements, which might lead to the assumption that insignificant changes in body size are to be expected in instar elements. Although our method assumes relative stability of instar body sizes, we observed an isolated significant size change within instar A-2 of *B. ottomanensis* (Fig. 5). This has no obvious ecological significance, but shows that significant fluctuations in instar body size can be observed with our method. However, in the case of sudden and extreme changes in body size, where individuals decrease to the size of the next smaller instar, our method would simply place these individuals in the smaller instar group. Forel *et al.* (2015) described this pattern of extreme dwarfing in two Permian–Triassic ostracod species of the genera *Basslerella* and *Bairdia*, which we think might have been inferred by the methodology. Despite the small sample size, especially in the upper section studied (Early Triassic), they consistently classified the largest occurring instars as adults and the smaller groups as successively decreasing instars. Given the small sample size, we argue that the assumption of equal sampling of all instars in each time unit, and thus the observed body size pattern, is unlikely. In our data set, which has a much larger sample size over a longer time scale, adults are regularly sampled, although not at every horizon, and the adults of the two most abundant species have a constant body size (Fig. 5).

No TSR in the studied ostracod species

The instars of *B. ottomanensis* do not change in size (Fig. 5), nor track or correlate with diversity, temperature or δ^{13}C (Tables S3, S4). Putting aside the unlikely concerns about the instar classification method, and because most instars are sampled throughout (Fig. 2), this might indicate that the changes in the full species body size are more likely to be signs of changes in the abundance of instars (e.g. adults), rather than actual signs of morphological adaptation.

The stable body size of *F. obunca* (Fig. 5), the species that lived through the gradual warming leading up to the rapid temperature increase that culminates in the extinction, is probably the most notable result of this study. Due to the high degree of warming towards the extinction horizon in the Aras Valley section, we expected a correlating body size decrease in *F. obunca*, according to the TSR in ectotherms. However, the body size of *F. obunca* and its instars is stable and the most parsimonious model indicates, that the full species' body size only correlates slightly with diversity (Table S3), an effect that

disappears when testing for it in a single instar. The effect of diversity on the body size of *F. obunca* is also low and not significant, suggesting that the variables we used might generally be badly fit for explaining this species' body size. The lack of correlation with temperature could lead to the assumption that *F. obunca* was simply not at all sensitive to the temperature increase in the end-Permian. Even though ostracods are known to be especially resilient to high temperatures (Wickstrom & Castenholz 1971; Song *et al.* 2014), they still experience large-scale extinction events during hyperthermal crises, including the end-Permian (e.g. Crasquin & Forel 2014). Certain factors may have helped buffer species against the damaging effects of warming. For example, *F. obunca* might have been protected from shrinking, if its ecological niche was especially broad (Deutsch *et al.* 2022). But even in ecologically specialized organisms, oxygen supply, as well as nutrition are limiting factors for growth during warming intervals. If the organism can increase its nutrient intake according to its increased demand through warming increased metabolism, it may be able to offset the warming-induced growth limitations (Sheridan & Bickford 2011). This might be a possibility in the Aras Valley section, as there are no signs of hypoxic conditions or a pre-extinction carbon cycle collapse during the end-Permian. However, even if the species might have been somewhat protected from catastrophic effects, we reject the assumption that *F. obunca* was resistant to the increasing temperatures, as the species becomes regionally extinct along with the other ostracod species at the extinction horizon (Gliwa *et al.* 2021).

All aspects considered, we conclude that *F. obunca* was probably sensitive to the vastly increasing temperatures, but that its adaptation strategy might not have included processes that result in a decreased body size. This could possibly point toward a process seen in experimental studies on some modern ostracods. These benthic ostracods show no decrease in the body size of instars, but instead an accelerated growth between developmental stages as a typical response to increasing ambient temperatures (Aguilar-Alberola 2013; Liberto *et al.* 2014). However, even though we consider this to be a possible scenario, testing it is unfortunately not possible using fossil ostracod data.

CONCLUSION

This is the first quantitative study directly relating fossil ostracod body sizes with their ambient temperature instead of vaguely indicative regional or global temperature proxies, to test for the presence of the TSR. Our results suggest that ostracods across the end-Permian Aras Valley section in Iran do not decrease in body size, both

inter- and intraspecifically. Instead, ostracod species with larger individuals settle shortly after the end-Permian mass extinction. We do not interpret this as a sign of immunity to thermal stress, as ostracods did experience an extinction event when temperatures reached a certain level. Instead, we discuss how the ostracods in this location might be exceptions to the TSR, instead using a mechanism to cope with thermal stress which does not involve a reduction in body size. A similar process can be observed in several recent experimental ostracod studies. Our results clearly show that the TSR is not as general as previously assumed, and that the ostracods in the Aras Valley section in Iran are an example of an exception to the rule. To find out whether the shrinking response of certain marine ecto-therms can be used as a proxy for deteriorating environmental conditions, including warming, we need to further investigate patterns in traits that determine, which organisms show this specific morphological adaptation to warming and which do not. Gaining this knowledge will be vital for the proper interpretation of early warning signs for catastrophic climate impacts in the marine realm.

Author contributions. **Conceptualization** PS Nätscher (PSN), D Korn (DK), K De Baets (KDB); **Data Curation** PSN; **Formal Analysis** PSN; **Funding Acquisition** PSN, DK, KDB, A Ghaderi (AG); **Investigation** J Gliwa (JG), PSN; **Methodology** PSN, DK, KDB; **Project Administration** PSN, DK, KDB; **Resources** JG, AG, DK; **Software** PSN; **Supervision** DK, KDB; **Validation** PSN, DK, KDB, JG, AG; **Visualization** PSN; **Writing – Original Draft Preparation** PSN; **Writing – Review & Editing** PSN, JG, AG, DK, KDB.

DATA ARCHIVING STATEMENT

Data, R code for statistical analyses and supplementary material for this study are available in the Dryad Digital Repository: https://doi.org/10.5061/dryad.xgxd254mb.

Editor. Yue Wang

SUPPORTING INFORMATION

Additional Supporting Information can be found online (https://doi.org/10.1111/pala.12667):

Figure S1. Instar classification plots (length × height) of the most parsimonious Gaussian mixture model (VEI) from the R package mclust, and BIC plots of all tested models.

Figure S2. Sedimentary profile of the Aras Valley section (northwest Iran) with: A, loess-smoothed mean calculated temperature derived from oxygen isotope measurements of the ostracod carapaces with the red shading representing the loess-smoothed SD; B, $\delta^{13}C$ curve that was reverse-engineered from Gliwa *et al.* (2022); C, corrected-in-bin diversity (Alroy 2008); D–H, loess-smoothed median body size curves for the raw body size data of the: D, full assemblage; E, Order Podocopida; F, Order Platycopida; G, enus *Fabalicypris*; H, species body size of *B. ottomanensis* and *F. obunca*.

Figure S3. Correlation plot of the three variables intended for use in the general least square (gls) models ($\delta^{13}C$, temperature, corrected in-bin-diversity).

Figure S4. Histograms of instar abundances within the 18 ostracod species (n > 9) for which we classified instar clusters with the Gaussian mixture modelling method in the R package mclust.

Figure S5. Boxplot of the body sizes of the species from the post-extinction assemblage, showing that six of them are larger than most of the other species in this assemblage.

Table S1. Methodology of the Rego Approach (Rego *et al.* 2012).

Table S2. AIC selection process of the autoregressive and moving average variables for the generalized least squares models to correct for temporal autocorrelation.

Table S3. Model results of the generalized least squares models, correcting for temporal autocorrelation, for the full assemblage, *F. obunca* and *B. ottomanensis*, as well as a subset of only the A-1 instar grouping for each of these, testing the influence of temperature and diversity on body size.

Table S4. Model results from the time series trend analyses (with the R package paleoTS) for the six instars of *B. ottomanensis*.

Table S5. Model results from the time series trend analyses (with the R package paleoTS) for the five instars of *F. obunca*.

Table S6. Posthoc Tukey HSD of ANOVA results between body sizes of the 12 species from the post-extinction assemblage of podocopids that dominates in the Aras Valley section between 0.01 m and 0.50 m above the extinction horizon.

REFERENCES

AGUILAR-ALBEROLA, J. A. 2013. *Heterocypris bosniaca* (Petkowski et al., 2000): Ecología y ontogenia de un ostrácodo (Crustacea: Ostracoda) de pozas temporales. Chapter 3: Breaking the temperature-size rule: thermal effects on growth, development and fecundity of a crustacean from temporary waters. PhD thesis, Universitat de València, pp. 71–92.

ALROY, J. 2008. Dynamics of origination and extinction in the marine fossil record. *Proceedings of the National Academy of Sciences*, **105**, 11536–11542.

ANGILLETTA, M. J., STEURY, T. D. and SEARS, M. W. 2004. Temperature, growth rate, and body size in ectotherms: fitting pieces of a life-history puzzle. *Integrative & Comparative Biology*, **44**, 498–509.

ATKINSON, D. 1994. Temperature and organism size: a biological law for organisms? *Advances in Ecological Research*, **25**, 1–58.

ATKINSON, D. and SIBLY, R. M. 1997. Why are organisms usually bigger in colder environments? Making sense of a life history puzzle. *Trends in Ecology & Evolution*, **12**, 235–239.

BOOMER, I., HORNE, D. J. and SLIPPER, I. J. 2003. The use of ostracods in palaeoenvironmental studies, or what can you do with an ostracod shell? *The Paleontological Society Papers*, **9**, 153–180.

BRAND, U. and VEIZER, J. 1981. Chemical diagenesis of a multicomponent carbonate system; 2, stable isotopes. *Journal of Sedimentary Research*, **51**, 987–997.

BRANDÃO, S. N. and HORNE, D. J. 2009. The platycopid signal of oxygen depletion in the ocean: a critical evaluation of the evidence from modern ostracod biology, ecology and depth distribution. *Palaeogeography, Palaeoclimatology, Palaeoecology*, **283**, 126–133.

BROWN, J. H. and MAURER, B. A. 1986. Body size, ecological dominance and Cope's rule. *Nature*, **324**, 248–250.

BURGESS, S. D., MUIRHEAD, J. D. and BOWRING, S. A. 2017. Initial pulse of Siberian Traps sills as the trigger of the end-Permian mass extinction. *Nature Communications*, **8**, 1–4.

CALOSI, P., PUTNAM, H. M., TWITCHETT, R. J. and VERMANDELE, F. 2019. Marine metazoan modern mass extinction: improving predictions by integrating fossil, modern, and physiological data. *Annual Review of Marine Science*, **11**, 20.1–20.22.

CHU, D., TONG, J., SONG, H. H., BENTON, M. J., SONG, H. H., YU, J., QIU, X., HUANG, Y. and TIAN, L. 2015a. Lilliput effect in freshwater ostracods during the Permian–Triassic extinction. *Palaeogeography, Palaeoclimatology, Palaeoecology*, **435**, 38–52.

CHU, D., TONG, J., SONG, H., BENTON, M. J., SONG, H., YU, J., QIU, X., HUANG, Y. and TIAN, L. 2015b. Reply to the comment on Chu et al., 'Lilliput effect in freshwater ostracods during the Permian-Triassic extinction' [Palaeogeography, Palaeoclimatology, Palaeoecology 435 (2015): 38–52]. *Palaeogeography, Palaeoclimatology, Palaeoecology*, **440**, 863–865.

CLARKSON, M. O., KASEMANN, S. A., WOOD, R. A., LENTON, T. M., DAINES, S. J., RICHOZ, S., OHNE-MUELLER, F., MEIXNER, A., POULTON, S. W. and TIPPER, E. T. 2015. Ocean acidification and the Permo-Triassic mass extinction. *Science*, **348**, 229–232.

CRASQUIN, S. and FOREL, M.-B. 2014. Ostracods (Crustacea) through Permian–Triassic events. *Earth-Science Reviews*, **137**, 52–64.

CRASQUIN-SOLEAU, S. and KERSHAW, S. 2005. Ostracod fauna from the Permian–Triassic boundary interval of South China (Huaying Mountains, eastern Sichuan Province): palaeoenvironmental significance. *Palaeogeography Palaeoclimatology Palaeoecology*, **217**, 131–141.

CRAWLEY, M. 2007. *The R book*. Wiley.

CRONIN, T. M., KAMIYA, T., DWYER, G. S., BELKIN, H., VANN, C. D., SCHWEDE, S. and WAGNER, R. 2005. Ecology and shell chemistry of *Loxoconcha matagordensis*. *Palaeogeography, Palaeoclimatology, Palaeoecology*, **225**, 14–67.

DAUFRESNE, M., LENGFELLNER, K. and SOMMER, U. 2009. Global warming benefits the small in aquatic ecosystems. *Proceedings of the National Academy of Sciences*, **106**, 12788–12793.

DE BAETS, K., JAROCHOWSKA, E., BUCHWALD, S. Z., KLUG, C. and KORN, D. 2022. Lithology controls ammonoid size distributions. *PALAIOS*, **37**, 744–754.

DEUTSCH, C., PENN, J. L., VERBERK, W. C. E. P., INOMURA, K., ENDRESS, M. G. and PAYNE, J. L. 2022. Impact of warming on aquatic body sizes explained by metabolic scaling from microbes to macrofauna. *Proceedings of the National Academy of Sciences*, **119**, 1–9.

DORMANN, C. F., ELITH, J., BACHER, S., BUCHMANN, C., CARL, G., CARRÉ, G., MARQUÉZ, J. R. G., GRUBER, B., LAFOURCADE, B., LEITÃO, P. J., MÜNKEMÜLLER, T., McCLEAN, C., OSBORNE, P. E., REINEKING, B., SCHRÖDER, B., SKIDMORE, A. K., ZURELL, D. and LAUTENBACH, S. 2013. Collinearity: a review of methods to deal with it and a simulation study evaluating their performance. *Ecography*, **36**, 27–46.

FENG, Y., SONG, H. and BOND, D. P. G. 2020. Size variations in foraminifers from the early Permian to the Late Triassic: implications for the Guadalupian–Lopingian and the Permian–Triassic mass extinctions. *Paleobiology*, **46**, 511–532.

FOREL, M. B. 2013. The Permian–Triassic mass extinction: Ostracods (Crustacea) and microbialites. *Comptes Rendus Geoscience*, **345**, 203–211.

FOREL, M. B. and CRASQUIN, S. 2015. Comment on the Chu et al., paper 'Lilliput effect in freshwater ostracods during the Permian–Triassic extinction' [Palaeogeography, Palaeoclimatology, Palaeoecology 435 (2015): 38–52]. *Palaeogeography, Palaeoclimatology, Palaeoecology*, **440**, 860–862.

FOREL, M. B., CRASQUIN, S., KERSHAW, S. and COLLIN, P. Y. 2013. In the aftermath of the end-Permian extinction: the microbialite refuge? *Terra Nova*, **25**, 137–143.

FOREL, M. B., CRASQUIN, S., CHITNARIN, A., ANGIOLINI, L. and GAETANI, M. 2015. Precocious sexual dimorphism and the Lilliput effect in Neo-Tethyan Ostracoda (Crustacea) through the Permian-Triassic boundary. *Palaeontology*, **58**, 409–454.

FOREL, M. B., TEKIN, U. K., OKUYUCU, C., BEDI, Y., TUNCER, A. and CRASQUIN, S. 2019. Discovery of a long-term refuge for ostracods (Crustacea) after the end-Permian extinction: a unique Carnian (Late Triassic) fauna from the Mersin Mélange, southern Turkey. *Journal of Systematic Palaeontology*, **17**, 9–58.

FOSTER, W. J., HEINDEL, K., RICHOZ, S., GLIWA, J., LEHRMANN, D. J., BAUD, A., KOLAR-JURKOVŠEK, T., ALJINOVIĆ, D., JURKOVŠEK, B., KORN, D., MARTINDALE, R. C. and PECKMANN, J. 2020. Suppressed competitive exclusion enabled the proliferation of Permian/Triassic boundary microbialites. *Depositional Record*, **6**, 62–74.

FRALEY, C., RAFTERY, A. E., SCRUCCA, L., MURPHY, T. B. and FOP, M. 2022. mclust: Gaussian mixture modelling ofr model-based clustering, classification, and density estimation. R package v.6.0.0. https://cran.r-project.org/package=mclust

FRIESENBICHLER, E., RICHOZ, S., BAUD, A., KRYSTYN, L., SAHAKYAN, L., VARDANYAN, S., PECKMANN, J., REITNER, J. and HEINDEL, K. 2018. Sponge-microbial build-ups from the lowermost Triassic Chanakhchi section in southern Armenia: microfacies and stable carbon isotopes. *Palaeogeography, Palaeoclimatology, Palaeoecology*, **490**, 653–672.

GHADERI, A. 2014. Stratigraphy and paleoecology of the Upper Permian to Permian – Triassic boundary in the northwest of Iran based on biostratigraphic data of conodonts and brachiopods. PhD thesis, Ferdowsi University of Mashhad, Iran, 488 pp. [in Farsi].

GHADERI, A., LEDA, L., SCHOBBEN, M., KORN, D. and ASHOURI, A. R. 2014. High-resolution stratigraphy of the Changhsingian (Late Permian) successions of NW Iran and the Transcaucasus based on lithological features, conodonts and ammonoids. *Fossil Record*, **17**, 41–57.

GLIWA, J., GHADERI, A., LEDA, L., SCHOBBEN, M., TOMÁS, S., FOSTER, W. J., FOREL, M. B., GHANIZADEH TABRIZI, N., GRASBY, S. E., STRUCK, U., REZA ASHOURI, A. and KORN, D. 2020. Aras Valley (northwest Iran): high-resolution stratigraphy of a continuous central Tethyan Permian-Triassic boundary section. *Fossil Record*, **23**, 33–69.

GLIWA, J., FOREL, M. B., CRASQUIN, S., GHADERI, A. and KORN, D. 2021. Ostracods from the end-Permian mass extinction in the Aras Valley section (north-west Iran). *Papers in Palaeontology*, **7**, 1003–1042.

GLIWA, J., WIEDENBECK, M., SCHOBBEN, M., ULLMANN, C. V., KIESSLING, W., GHADERI, A., STRUCK, U. and KORN, D. 2022. Gradual warming prior to the end-Permian mass extinction. *Palaeontology*, **65**, e12621.

GRO, J. 2010. *Grundlegende Statistik mit R: Eine anwendungsorientierte Einführung in die Verwendung der Statistik Software R*. Vieweg+Teubner Verlag.

HE, W., SHI, G. R., FENG, Q., CAMPI, M. J., GU, S., BU, J., PENG, Y. and MENG, Y. 2007. Brachiopod miniaturization and its possible causes during the Permian-Triassic crisis in deep water environments, South China. *Palaeogeography, Palaeoclimatology, Palaeoecology*, **252**, 145–163.

HEINDEL, K., FOSTER, W. J., RICHOZ, S., BIRGEL, D., RODEN, V. J., BAUD, A., BRANDNER, R., KRYSTYN, L., MOHTAT, T., KOSUN, E., TWITCHETT, R. J., REITNER, J. and PECKMANN, J. 2018. The formation of microbial-metazoan bioherms and biostromes following the latest Permian mass extinction. *Gondwana Research*, **61**, 187–202.

HOLM, S. 1979. A simple sequentially rejective multiple test procedure. *Scandinavian Journal of Statistics*, **6** (2), 65–70.

HORNE, D. J., BRANDÃO, S. N. and SLIPPER, I. J. 2011. The platycopid signal deciphered: responses of ostracod taxa to environmental change during the Cenomanian–Turonian Boundary Event (Late Cretaceous) in SE England. *Palaeogeography, Palaeoclimatology, Palaeoecology*, **308**, 304–312.

HUNT, G. 2019. paleoTS: analyze paleontological time-series. R package v.0.5.2. https://cran.r-project.org/package=paleoTS

HUNT, G. and CHAPMAN, R. E. 2001. Evaluating hypotheses of instar-grouping in arthropods: a maximum likelihood approach. *Paleobiology*, **27**, 466–484.

HUNT, G. and ROY, K. 2006. Climate change, body size evolution, and Cope's Rule deep-sea ostracodes. *Proceedings of the National Academy of Sciences*, **103**, 1347–1352.

HUNT, G., WICAKSONO, S. A., BROWN, J. E. and MacLEOD, K. G. 2010. Climate-driven body-size trends in the ostracod fauna of the deep Indian Ocean. *Palaeontology*, **53**, 1255–1268.

JOACHIMSKI, M. M., LAI, X., SHEN, S., JIANG, H., LUO, G., CHEN, B., CHEN, J. and SUN, Y. 2012. Climate warming in the latest Permian and the Permian–Triassic mass extinction. *Geology*, **40**, 195–198.

JOACHIMSKI, M. M., ALEKSEEV, A. S., GRIGORYAN, A. and GATOVSKY, Y. A. 2022. Siberian Trap volcanism, global warming and the Permian Triassic mass extinction: new insights from Armenian Permian-Triassic sections: Reply. *Bulletin of the Geological Society of America*, **134**, 1087–1088.

JURIKOVA, H., GUTJAHR, M., WALLMANN, K., FLÖGEL, S., LIEBETRAU, V., POSENATO, R., ANGIOLINI, L., GARBELLI, C., BRAND, U., WIEDENBECK, M. and EISENHAUER, A. 2020. Permian–Triassic mass extinction pulses driven by major marine carbon cycle perturbations. *Nature Geoscience*, **13**, 745–750.

KAMIYA, T. 1988. Contrasting population ecology of two species of *Loxoconcha* (Ostracoda, Crustacea) in Recent Zostera (eelgrass) beds: adaptive differences between phytal and bottom-dwelling species. *Micropaleontology*, **34**, 316–331.

KIESSLING, W., SCHOBBEN, M., GHADERI, A., HAIRAPETIAN, V., LEDA, L. and KORN, D. 2018. Pre-mass extinction decline of latest Permian ammonoids. *Geology*, **46**, 283–286.

KIESSLING, W., SMITH, J. A. and RAJA, N. B. 2023. Improving the relevance of paleontology to climate change policy. *Proceedings of the National Academy of Sciences*, **120**, e2201926119.

KIM, S. T. and O'NEIL, J. R. 1997. Equilibrium and nonequilibrium oxygen isotope effects in synthetic carbonates. *Geochimica et Cosmochimica Acta*, **61**, 3461–3475.

KINGSOLVER, J. G. and PFENNIG, D. W. 2004. Individual-level selection as a cause of Cope's rule of phyletic size increase. *Evolution*, **58**, 1608–1612.

KOCSIS, Á. T., REDDIN, C. J., ALROY, J. and KIESSLING, W. 2019. The R package divDyn for quantifying diversity dynamics using fossil sampling data. *Methods in Ecology & Evolution*, **10**, 735–743.

KOCSIS, A. T., ALROY, J., REDDIN, C. J. and KIESSLING, W. 2021. divDyn: diversity dynamics using fossil sampling data. R package v.0.801. https://cran.r-project.org/package=divDyn

KÖNIGSHOF, P. 1992. Der Farbänderungsindex von Conodonten (CAI) in paläozoischen-Gesteinen (Mitteldevon bis Unterkarbon) des Rheinischen-Schiefergebirges. *Courier Forschungsinstitut Senckenberg*, **146**, 1–118.

KORDAS, R. L., HARLEY, C. D. G. and O'CONNOR, M. I. 2011. Community ecology in a warming world: the influence of temperature on interspecific interactions in marine systems. *Journal of Experimental Marine Biology & Ecology*, **400**, 218–226.

LATIFA, G. A. 1987. Effect of temperature on the development of embryonic and postembryonic stages of *Heterocypris incongruens* (Ramdohr 1808) (Ostracoda). *Crustaceana*, **52**, 95–100.

LEDA, L., KORN, D., GHADERI, A., HAIRAPETIAN, V., STRUCK, U. and REIMOLD, W. U. 2014. Lithostratigraphy and carbonate microfacies across the Permian–Triassic boundary near Julfa (NW Iran) and in the Baghuk Mountains (Central Iran). *Facies*, **60**, 295–325.

LIBERTO, R., CÉSAR, I. I. and MESQUITA-JOANES, F. 2014. Postembryonic growth in two species of freshwater Ostracoda (Crustacea) shows a size-age sigmoid model fit and temperature effects on development time, but no clear temperature-size rule (TSR) pattern. *Limnology*, **15**, 57–67.

LUO, G., LAI, X., JIANG, H. and ZHANG, K. 2006. Size variation of the end Permian conodont *Neogondolella* at Meishan Section, Changxing, Zhejiang and its significance. *Science in China, Series D: Earth Sciences*, **49**, 337–347.

LUO, G., LAI, X., SHI, G. R., JIANG, H., YIN, H., XIE, S., TONG, J., ZHANG, K., HE, W. and WIGNALL, P. B. 2008. Size variation of conodont elements of the *Hindeodus-Isarcicella* clade during the Permian–Triassic transition in South China and its implication for mass extinction. *Palaeogeography, Palaeoclimatology, Palaeoecology*, **264**, 176–187.

MAGNUSSON, A. 2022. areaplot: plot stacked areas and confidence bands as filled polygons. R package v.1.2.3. https://cran.r-project.org/package=areaplot

MAJORAN, S., AGRENIUS, S. and KUCERA, M. 2000. The effect of temperature on shell size and growth rate in *Krithe praetexta praetexta* (Sars). *Hydrobiologia*, **419**, 141–148.

MARTENS, K. 1985. Effects of temperature and salinity on postembryonic growth in *Mytilocypris henricae* (Chapman) (Crustacea, Ostracoda). *The Crustacean Society*, **5**, 258–272.

MELNYK, D. H. and MADDOCKS, R. F. 1988. Ostracode biostratigraphy of the Permo-Carboniferous of central and north-central Texas, Part II: ostracode zonation. *Micropaleontology*, **34**, 21–40.

MUTTONI, G., MATTEI, M., BALINI, M., ZANCHI, A., GAETANI, M. and BERRA, F. 2009a. The drift history of Iran from the Ordovician to the Triassic. *Geological Society Special Publication*, **312**, 7–29.

MUTTONI, G., GAETANI, M., KENT, D. V., SCIUNNACH, D., ANGIOLINI, L., BERRA, F., GARZANTI, E., MATTEI, M. and ZANCHI, A. 2009b. Opening of the Neo-Tethys ocean and the Pangea B to Pangea A transformation during the Permian. *GeoArabia*, **14**, 17–48.

NÄTSCHER, P. S., DERA, G., REDDIN, C. J., RITA, P. and DE BAETS, K. 2021. Morphological response accompanying size reduction of belemnites during an Early Jurassic hyperthermal event modulated by life history. *Scientific Reports*, **11**, 1–11.

NÄTSCHER, P. S., GLIWA, J., DE BAETS, K., GHADERI, A. and KORN, D. 2023. Data from: Exceptions to the temperature-size rule: no Lilliput Effect in end-Permian ostracods (Crustacea) from Aras Valley (NW Iran). Dryad Digital Repository. https://doi.org/10.5061/dryad.xgxd254mb

OHLBERGER, J. 2013. Climate warming and ectotherm body size – from individual physiology to community ecology. *Functional Ecology*, **27**, 991–1001.

PAYNE, J. L. and CLAPHAM, M. E. 2012. End-Permian mass extinction in the oceans: an ancient analog for the twenty-first century? *Annual Review of Earth & Planetary Sciences*, **40**, 89–111.

PINHEIRO, J., BATES, D., DEBROY, S., SARKAR, D., HEISTERKAMP, S., VAN WILLIGEN, B. and RANKE, J. 2021. nlme: linear and nonlinear mixed effects models. R package v.3.1-157. https://cran.r-project.org/package=nlme

POLOCZANSKA, E. S., BURROWS, M. T., BROWN, C. J., MOLINOS, J. G., HALPERN, B. S., HOEGH-GULDBERG, O., KAPPEL, C. V., MOORE, P. J., RICHARDSON, A. J., SCHOEMAN, D. S. and SYDEMAN, W. J. 2016. Responses of marine organisms to climate change across oceans. *Frontiers in Marine Science*, **3**, 1–21.

R CORE TEAM. 2013. R: a language and environment for statistical computing. R Foundation for Statistical Computing. https://www.R-project.org

REDDIN, C. J., KOCSIS, Á. T. and KIESSLING, W. 2018. Marine invertebrate migrations trace climate change over 450 million years. *Global Ecology & Biogeography*, **27**, 704–713.

REGO, B. L., WANG, S. C., ALTINER, D. and PAYNE, J. L. 2012. Within- and among-genus components of size evolution during mass extinction, recovery, and background intervals: a case study of Late Permian through Late Triassic foraminifera. *Paleobiology*, **38**, 627–643.

RITA, P., NÄTSCHER, P., DUARTE, L. V., WEIS, R. and DE BAETS, K. 2019. Mechanisms and drivers of belemnite body-size dynamics across the Pliensbachian–Toarcian crisis. *Royal Society Open Science*, **6**, 190494.

ROHATGI, A. 2022. WebPlotDigitizer v.4.6. https://automeris.io/WebPlotDigitizer

SCHOBBEN, M., FOSTER, W. J., SLEVELAND, A. R. N., ZUCHUAT, V., SVENSEN, H. H., PLANKE, S., BOND, D. P. G., MARCELIS, F., NEWTON, R. J., WIGNALL, P. B. and POULTON, S. W. 2020. A nutrient control on marine anoxia during the end-Permian mass extinction. *Nature Geoscience*, **13**, 640–646.

SCHOBBEN, M., JOACHIMSKI, M. M., KORN, D., LEDA, L. and KORTE, C. 2014. Palaeotethys seawater temperature rise and an intensified hydrological cycle following the end-Permian mass extinction. *Gondwana Research*, **26**, 675–683.

SCRUCCA, L., FOP, M., MURPHY, T. B. and RAFTERY, A. E. 2016. mclust 5: clustering, classification and density estimation using Gaussian finite mixture models. *The R Journal*, **8**, 289–317.

SEPKOSKI, J. J. Jr 1984. A kinetic model of Phanerozoic taxonomic diversity. III. Post-Paleozoic families and mass extinctions. *Paleobiology*, **10**, 246–267.

SEPKOSKI, J. J. Jr BAMBACH, R. K., RAUP, D. M. and VALENTINE, J. M. 1981. Phanerozoic marine diversity and the fossil record. *Nature*, **293**, 435–437.

SHERIDAN, J. A. and BICKFORD, D. 2011. Shrinking body size as an ecological response to climate change. *Nature Climate Change*, **1**, 401–406.

SONG, H., TONG, J. and CHEN, Z. Q. 2011. Evolutionary dynamics of the Permian–Triassic foraminifer size: evidence for Lilliput effect in the end-Permian mass extinction and its aftermath. *Palaeogeography, Palaeoclimatology, Palaeoecology*, **308**, 98–110.

SONG, H., WIGNALL, P. B., CHU, D., TONG, J., SUN, Y., SONG, H., HE, W. and TIAN, L. 2014. Anoxia/high temperature double whammy during the Permian-Triassic marine crisis and its aftermath. *Scientific Reports*, **4**, 1–7.

STAMPFLI, G. M. and BOREL, G. D. 2002. A plate tectonic model for the Paleozoic and Mesozoic constrained by dynamic plate boundaries and restored synthetic oceanic isochrons. *Earth & Planetary Science Letters*, **196**, 17–33.

STAMPFLI, G. M. and BOREL, G. D. 2004. The TRANSMED transects in space and time: constraints on the paleotectonic evolution of the Mediterranean domain. 53–90. *In* CAVAZZA, W., ROURE, F., SPAKMAN, W., STAMPFLI, G. M. and ZIEGLER, P. A. (eds) *The TRANSMED Atlas: The Mediterranean Region from crust to mantle*. Springer Verlag.

STANLEY, S. M. 2016. Estimates of the magnitudes of major marine mass extinctions in earth history. *Proceedings of the National Academy of Sciences*, **113**, E6325–E6334.

SUN, Y., JOACHIMSKI, M. M., WIGNALL, P. B., YAN, C., CHEN, Y., JIANG, H., WANG, L. and LAI, X. 2012. Lethally hot temperatures during the Early Triassic greenhouse. *Science*, **338**, 366–370.

TWITCHETT, R. J. 2007. The Lilliput effect in the aftermath of the end-Permian extinction event. *Palaeogeography, Palaeoclimatology, Palaeoecology*, **252**, 132–144.

URBANEK, A. 1993. Biotic crises in the history of Upper Silurian graptoloids: a palaeobiological model. *Historical Biology*, **7**, 29–50.

WAGENMAKERS, E. and FARRELL, S. 2004. AIC model selection using Akaike weights. *Psychonomic Bulletin & Review*, **11**, 192–196.

WEI, T. and SIMKO, V. 2021. corrplot: visualization of a correlation matrix. R package v.0.92. https://cran.r-project.org/package=corrplot

WHATLEY, R. 1991. The platycopid signal: a means of detecting kenoxic events using Ostracoda. *Journal of Micropalaeontology*, **10**, 181–185.

WICKSTROM, C. E. and CASTENHOLZ, R. W. 1971. Thermophilic ostracod: aquatic metazoan with the highest known temperature tolerance. *Science*, **181**, 1063–1064.

YAMAGUCHI, T., NORRIS, R. D. and BORNEMANN, A. 2012. Dwarfing of ostracodes during the Paleocene–Eocene Thermal Maximum at DSDP Site 401 (Bay of Biscay, North Atlantic) and its implication for changes in organic carbon cycle in deep-sea benthic ecosystem. *Palaeogeography, Palaeoclimatology, Palaeoecology*, **346–347**, 130–144.

ZHANG, Y., SHI, G. R., HE, W. H., WU, H. T., LEI, Y., ZHANG, K. X., DU, C. C., YANG, T. L., YUE, M. L. and XIAO, Y. F. 2016. Significant pre-mass extinction animal body-size changes: evidences from the Permian–Triassic boundary brachiopod faunas of South China. *Palaeogeography, Palaeoclimatology, Palaeoecology*, **448**, 85–95.